Momentum vector correlation maps for three-particle fragmentation of neutral triatomic hydrogen near its ionization threshold

Peer Fechner and Hanspeter Helm
Department of Molecular and Optical Physics, Albert-Ludwigs-Universität, Hermann-Herder Strasse 3, D-79104 Freiburg, Germany
(Received 10 August 2010; published 29 November 2010)

Three-particle dissociation of high-lying Rydberg states of H_3, in the immediate vicinity of the ionization threshold, is induced by an external electric field. We observe that the momentum vector correlation map of the center-of-mass motion of the fragments changes rapidly with electronic energy. Near- and above-threshold substantial contributions of fragment orientations which are characteristic of near-linear geometry appear, i.e., two atoms with opposing momenta, the third atom being nearly at rest. This finding is similar to observations by Strasser *et al.* [Phys. Rev. A **66**, 032719 (2002)], who studied dissociative recombination of cold H_3^+ ions with slow electrons. We discuss the likely dissociation paths responsible for the observed correlation.

DOI: 10.1103/PhysRevA.82.052523 PACS number(s): 33.15.Fm, 31.50.Gh, 33.80.Gj, 34.50.Lf

I. INTRODUCTION

Motivated in part by the importance of dissociative recombination of H_3^+ with slow electrons [1,2] in astrophysics, processes leading to the fragmentation of the neutral triatomic hydrogen molecule have been subject to intense study. Experiments have been refined to trace the final state distribution emerging in the dissociation of the molecule. Specifically the distribution of total energy among translational and internal degrees of freedom in the reaction [3–5]

$$H_3^* \rightarrow H(1s) + H_2(v, J) \tag{1}$$

and among the translational degrees of freedom in three-particle decay [3,4,6–9]

$$H_3^* \rightarrow H(1s) + H(1s) + H(1s) \tag{2}$$

has been studied. While remarkable agreement between theory and experiment [10] has been achieved for the vibrational distributions in reaction (1), the subtle dynamics involved in reaction (2) is not fully understood at this point. First attempts to clarify the dynamics and to predict the momentum vector correlation (MVC) maps for reaction (2) have recently been made by Lehner and Jungen [11] and by Galster [12]. These authors treat predissociation of the lowest $2s$ Rydberg levels of H_3 and they predict certain features which appear in the corresponding experimental MVC maps. Experiments [9] reveal increasing complexity of the maps when moving to higher-lying Rydberg states as well as an increasing contribution of fragmentation patterns where, in center-of-mass geometry, two atoms have antiparallel momentum vectors, the third atom being nearly at rest. In the following we refer to this configuration as *near-linear geometry*. An experimental MVC map has also been obtained in dissociative recombination (DR) at the Test Storage Ring in Heidelberg [6]. In this experiment vibrationally cold molecular ions were merged with slow electrons and MVC maps inferred[1] from the spatial fragmentation pattern. This rather different experiment and method of analysis also points to a dominance of fragment orientations in near-linear geometries.

It is now generally accepted that the rapid dissociative recombination of H_3^+ ions with slow electrons involves capture into Rydberg states. Among these the npe' states[2] diabatically connect to the dissociative ground state through Jahn-Teller coupling between electronic and nuclear motion [13]. The cold molecular ion in the DR experiment is in equilateral triangular geometry. Thus it may at first appear surprising that fragments should appear with preference for near-linear orientation. However, the potential energy surfaces of Jungen[3] point to avoided crossings which can steer wave packets of D_{3h} geometry into the linear configuration, so at least a plausible argument exists for the experimental findings.

Here we discuss an experiment involving H_3 molecules in high-lying ($n \geqslant 6$) and long-lived Rydberg states, at energies in the immediate vicinity of the ionization limit. We force these molecules to dissociate by Stark-mixing them with more rapidly predissociating states. The MVC maps are observed to rapidly change with total energy. Near and above the ionization threshold, $H_3^+ + e$, preferred dissociation into near-linear fragment geometries occurs.

II. EXPERIMENT

Our experiment is performed with the fast-beam apparatus discussed previously [9,14–16]. It is modified by a spatially localized Stark-field section as shown schematically in Fig. 1.

Neutral H_3 molecules are produced in charge transfer of 3 keV H_3^+ ions in a cesium vapor cell. At the exit of the cell residual ions are deflected by a weak electric field. After passage through a 1-mm-diameter aperture fast neutral molecules reach the Stark-field section, 300 mm downstream from the charge transfer cell. The field electrodes are two razor blades, spaced by 2 mm. The field is terminated by grounded plates, at a distance of 1.5 mm from the electrodes. During

[1] In contrast to our detection system, no timing information of the correlated fragments is collected. By applying a Monte Carlo reconstruction method, the authors derived a MVC map from the projected spatial fragmentation pattern [6].

[2] According to irreducible representations of the group C_{3v} the notation e' signifies the two degenerate states of a p orbital lying in the nuclear plane, with n giving the principal quantum number of the outer electron, $n \geqslant 2$.

[3] See Ref. [9], pp. 1–5.

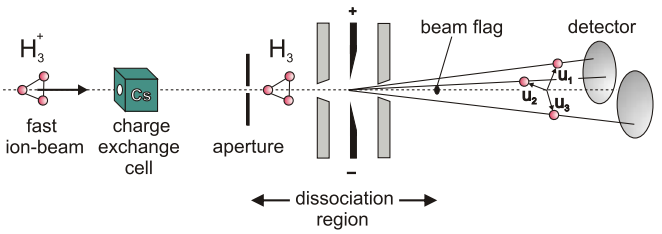

FIG. 1. Unimolecular dissociation of H_3^* is detected over the region from the aperture to the beam flag (length 115 mm), when no voltage is applied. Electric-field-induced dissociation is localized to the 3 mm region of the Stark electrodes which are shown on a greatly expanded scale here.

their ≈7 ns transit time through the Stark-field region, the molecules experience an inhomogenous dc field. Voltages of up to 7 kV can be applied between the electrodes. A beam flag intercepts undissociated molecules at a distance of 100 mm from the Stark-field region. Fragments from predissociation with sufficient transverse momentum pass this flag and reach the multihit coincidence detector after a free flight of 1170 mm (measured from the Stark field). Arrival times and positions of the three hydrogen atoms are registered by the detectors in coincidence with a spatial resolution of 60 μm and a temporal resolution of 25 ps. Knowing the spatial point of dissociation, the momentum vectors $\mathbf{u}_i$, and the kinetic energy of each atom in the center-of-mass frame, E_i with $i = 1$–3, can be determined from the coincidence data [17]. By summation the total kinetic energy release of process (2) is obtained, $W = \sum_i E_i$.

The charge-exchange process generates a wide spectrum of neutral states, most of which dissociate within a few nanoseconds, in the immediate vicinity of the charge-transfer cell and remain undetected. Molecules in the rotationless $2pA_2''$ ($N = 0, K = 0$) state are metastable [18] and they form the dominant contribution to the beam of neutral molecules which survive the time of flight to the Stark-field section. In addition to these molecules a tiny fraction of higher-lying Rydberg states are detected, as shown by the trace labeled 0 kV in Fig. 2. The broad range of apparent energies at which decays from these latter states appear in the energy spectrum derives from the statistical distribution of locations where the dissociation occurs along the beam path, all the way from just before the aperture to the position of the beam flag (see Fig. 1), a distance of about 100 mm.

When the Stark field is present, a substantial fraction of the molecules which suffer the weak unimolecular decay along the beam path can be forced to dissociate by electric-field-induced mixing in the Stark-field region. The field couples the long-lived Rydberg molecules to rapidly predissociating states, thereby localizing the space where molecules dissociate. As a consequence the energy release spectrum sharpens, concurrent with a substantial increase in dissociation events from Rydberg states near the ionization threshold. This is apparent from Fig. 2 which gives spectra at different field voltages. The ionization threshold, $H_3{}^+(N^+ = 1, K^+ = 1) + e$, lies at 4.787 eV above $H(1s) + H(1s) + H(1s)$; see the Appendix. For voltages greater than about 1 kV the spectral shape of the high-energy fragments saturates. Note the low count rates; about 10 molecules per minute are detected in the entire spectrum at

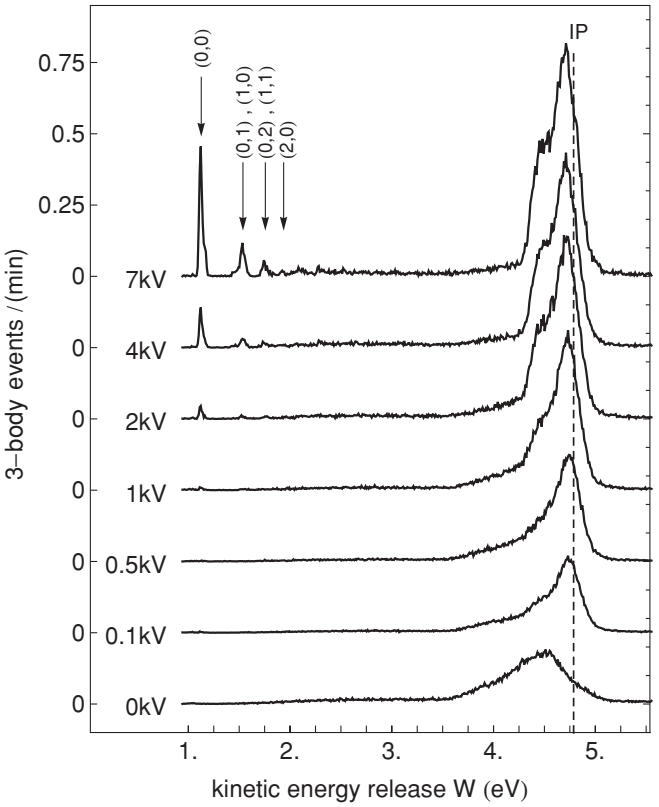

FIG. 2. Measured kinetic energy release W for the three-body decay at different applied Stark voltages. The energy values are calculated on the assumption that the distance from the point of dissociation to the detector is 1170 mm. The arrows indicate the energetic location of vibrational levels of metastable $2pA_2''$ molecules which are induced to dissociate by the Stark field. Vibrational excitations are given in the form (v_1,v_2), where the v_i give the quanta of excitation in the symmetric breathing and the degenerate bending vibration, respectively.

zero field, about 40 molecules per minute in the spectrum at 7 kV.

At high field strength the Stark field admixes substantial s character to molecules in the metastable state. As a consequence the dissociation of vibrational levels of $2pA_2''$ appear in the low-energy part of the fragment kinetic spectra at elevated values of the field. These are the peaks between 1 and 2 eV which are labeled by the vibrational excitation (see Fig. 2). Contributions from the $2sA_1'(0,0)$ molecules are absent due to the detector cutoff at 0.95 eV. It is apparent from the low-energy spectra that individual vibrational states are easily discernible at the energy resolution of our experiment. As the resolution is practically independent of the kinetic energy this points to the fact that the broad unresolved peak near the ionization threshold is a consequence of the high density of Rydberg states which contribute here.

III. RESULTS AND DISCUSSION

A. Origin of high-lying Rydberg states

Neutral H_3 molecules with principal quantum number n and angular momentum quantum number ℓ of the outer electron

are formed in the charge-transfer reaction

$$H_3^+ + Cs \rightarrow H_3(n,\ell) + Cs^+ + \Delta E, \quad (3)$$

where ΔE is the energy defect. Reaction (3) is weakly endothermic for the final state $2p\,A_2''(n=2,\ell=1)$ with $\Delta E = -0.221$ eV. The defect energy falls with rising values of n and reaches -3.89 eV for $n \rightarrow \infty$.

It appears reasonable to assume that the probability of electron capture into $H_3(n,\ell)$ orbitals scales with the inverse third power of the principal quantum number[4]

$$P_1 = c/n^3, \quad (4)$$

with c being a constant and to neglect effects of endothermicity. Our molecules take about 700 ns to travel from the charge-transfer cell to the dissociation region, hence only long-lived states can survive this passage. The probability of spontaneous emission of $H_3(n,\ell)$ decreases with increasing n and ℓ. We set for the probability of survival

$$P_2 = \exp[-t/\tau(n,\ell)]$$

and take as a scaling rule $\tau(n,\ell = n-1) = n^3/350\ \mu$s. This gives for the maximal ℓ values $\tau(7,6) = 0.98\ \mu$s and $\tau(6,5) = 0.62\ \mu$s, in good agreement with the lifetime of the corresponding hydrogenic states [19]. Molecular excited states have predissociation as an additional channel for decay. Information on unimolecular decay by predissociation is only available for states with $n \leqslant 4$, and sporadic windows of dissociation are known at certain higher n values of the H_3 molecule [20,21]. What we learn from the current experiment is that predissociation can be induced or at least enhanced by an electric field and that only states with $n \geqslant 6$ contribute significantly to the high-energy fragment spectrum of our experiment.

B. Model simulation

Using the product probability $P_1 P_2$ as a measure of abundance of each Rydberg state and assuming that only the longest-lived states, those with $\ell = n-1$, contribute to the field-induced spectrum, we simulate the observed distribution by summing over all Rydberg series which converge to the lowest rotational levels of the ground and first excited vibrational states of the molecular ion. The quantum defect of the Rydberg states is taken as zero and a rotational temperature of the parent ion[5] of $T = 1000$ K is assumed. Each individual Rydberg peak is folded with the experimental width which we observe in photodissociation of the laser-excited $3dE''(0,0)^0(N=1,K=1)$ level.[6] The result of the simulation is compared to the measurement recorded at 7 kV in Fig. 3. There are two free parameters in our simulation. One is the fractional population in vibrationally excited states. We know from previous experiments that the primary ion beam contains roughly 10% in vibrationally excited states. The signal at energies above the ionization threshold in Fig. 3 suggests that a significantly smaller fraction contributes to the field-induced dissociation spectrum. For the simulation we assumed a fractional population of only 2% in our simulation, not unreasonable in view that these states can autoionize. The second free parameter is the absolute count rate, controlled by the factor c of Eq. (4). We adjusted c to approximately equal the integrated counts in two spectra. The result of the simulation is shown by the full line in Fig. 3.

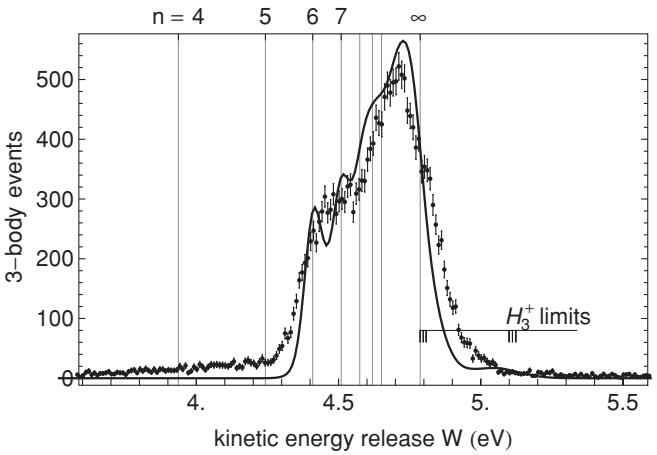

FIG. 3. The simulation of the spectrum is shown by the full line. Experimental data are shown with the statistical error bar. The spectrum was accumulated in an 11 h run. A potential energy difference of 7 kV was used. The ionization limits shown correspond to the lowest three rotational levels of the lowest two vibrational states of H_3^+. The top axis gives the Rydberg series with zero quantum defect, converging to the lowest rotational level of H_3^+.

Considering the simplicity of our model, the agreement between simulation and experiment is quite remarkable. The deviation at higher energies might be removed by introducing an n- and ℓ-dependent autoionization probability, but this appears unwarranted as no new insight would be obtained. The deviation at the lower-energy end likely arises from the finite dissociation lifetimes of the Stark-admixed states. A temporal delay in their dissociation to positions downstream from the Stark field leads to an apparent lower energy release. This is because the data analysis assumes a fixed distance of dissociation, 1170 mm from the detector surface. The spectra reveal a weak background of unimolecular decay which appears to be immune to the field strengths applied in our experiment. Contributions from Rydberg molecules with $n < 6$ are absent from the spectrum, an observation which points to the importance of high-ℓ states as origin for the fragment spectrum.

C. Low-lying Rydberg states

At Stark voltages larger than $\approx$1 kV the field-induced dissociation of the high Rydberg states begins to saturate, but individual peaks grow from the near-zero background at low energies, in the region between 1 and 2 eV, at yet higher field strength (see Fig. 2). These fragments originate from molecules in different vibrational levels of the metastable

[4]This argument is based on the volume occupied by the Rydberg orbital. The volume increases with n^3 and hence finds increasingly weaker overlap with that of the 5s electron of the cesium atom.

[5]Due to the large rotational spacing the result is only weakly dependent on temperature.

[6]The folding function is nearly a Gaussian with full width at half maximum of 110 meV.

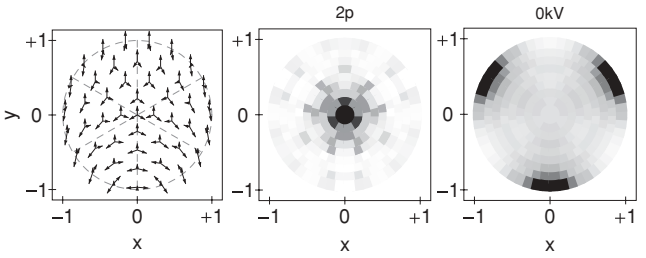

FIG. 4. Characteristic distributions of momentum vectors in a Dalitz map are shown on the left. The dimensionless coordinates are those of Eq. (5). The experimental result for the metastable molecule $2p\,A_2''(0,0)(N=0,K=0)$ is shown at the center. On the right the Dalitz map for all events in the energy interval 3.5–5.0 eV at zero electric field is shown. The gray scale is given in Fig. 5.

$2p\,A_2''$ state. The field mixes them with the nearby $2s^2\,A_1'$ levels which are rapidly predissociated, $\tau \approx 170$ fs [22]. We have examined this finding recently [16] for the lowest level visible in Fig. 2 and do not consider these peaks further but note that the flight distance to the detector in the current work was chosen for optimized detection of fragments with $W \geqslant 3$ eV. This severely suppresses the signal of peaks at $W < 2$ eV, practically cutting off the spectrum at fragment energies below 1 eV.

We have studied the fragmentation spectra in Fig. 2 with the electric field oriented parallel and perpendicular to the orientation of the two detector halves. We find that the low-energy peaks show a preferred alignment of the nuclear plane perpendicular to the electric field vector as has been noted in our previous experiment [16]. This observation can be understood in terms of the orientation of the $2p\,A_2''$ orbital perpendicular to the nuclear plane, electric-field-induced mixing being optimal when the p orbital is aligned parallel to the electric field vector. By contrast, our high-energy fragments (4.3–5 eV) show no such preferred alignment. This lends further support to our hypothesis that the molecules observed in field-induced predissociation are in high electronic angular momentum states.

D. Dalitz plots

The momentum vector correlation (MVC) in the final state, $H(1s) + H(1s) + H(1s)$, is the crucial result of our experiment. In order to represent the energy sharing among the three fragments of reaction (2), a Dalitz map [23] is most suitable. The Dalitz map indicates the center-of-mass arrangement of the fragment momentum vectors $m\mathbf{u}_i$ in the dissociation plane, with m being the mass of the neutral hydrogen atom. The coordinates of a MVC map,

$$x = 3(\varepsilon_2 - \varepsilon_1)/\sqrt{3} \quad \text{and} \quad y = 3(\varepsilon_3 - 1/3), \tag{5}$$

relate the reduced kinetic energy of the ith atom in the center-of-mass frame, $\varepsilon_i = m\mathbf{u}_i^2/(2W)$, to the orientation of the three momentum vectors. The quantities ε_i are normalized to the total energy release W. The latter quantity is determined for each molecule separately and serves to identify the initial state involved in dissociation. Due to momentum conservation, all experimental data fall inside a circle of radius 1. As we detect indistinguishable atoms the maps show sixfold symmetry.

The event position inside the circular area reflects the relative orientation of the momentum vectors of the three hydrogen atoms in the center-of-mass frame, as indicated in Fig. 4, left. The Dalitz map corresponding to the lowest-energy peak of the spectrum in Fig. 2 is shown in the center of Fig. 4. These are molecules in the vibrational ground state of the metastable molecule $2p\,A_2''$. These data [16] were obtained in a measurement optimized for detection of fragments with $W \approx 1$ eV. We have drawn the Dalitz plot in terms of circular segments of equal area, filled in gray color with the summed phase-space density of the corresponding area. The experimental phase space density of all Dalitz plots presented is corrected for the detection efficiency, which is obtained separately for each energy release by an appropriate Monte Carlo simulation.

Figure 5 gives Dalitz maps for the higher-energy fragments. Data recorded at different Stark voltages (0.5–7 kV) were added for improved statistics. The plots are sorted according

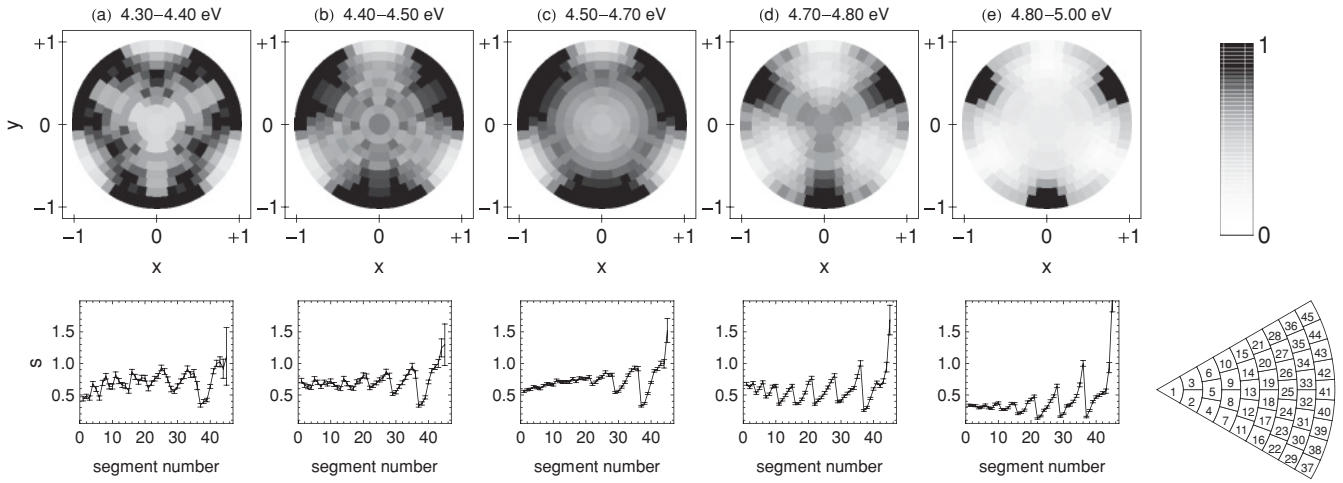

FIG. 5. Dalitz plots of fragments in specific energy intervals: W = (a)4.3–4.4 eV ($n = 6$), (b) 4.4–4.5 eV ($n = 7$), (c) 4.6–4.7 eV ($n = 8$–16), (d) 4.7–4.8 eV (around the ionization threshold), and (e) 4.8–5.0 eV (region of vibrational autoionization). The relative signal in each segment of a Dalitz plot is given in the lower row, together with the respective statistical error bars.

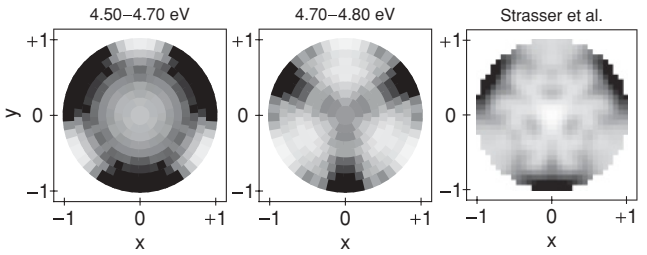

FIG. 6. Comparison of the result from Figs. 5(c) (left) and 5(d) (center) with the result of Strasser *et al.* [6] (right). The gray scale is that of Fig. 5.

to increasing energy W. Figure 5(a) refers to states with principal quantum number $n = 6$ while Fig. 5(b) refers to states with $n = 7$. Figure 5(c) shows states nominally $8 < n < 16$, Fig. 5(d) those with $n > 16$ to an energy of about 20 meV above threshold, while Fig. 5(e) covers the region of rotationally and vibrationally excited cores. Note that all states above 4.787 eV can in principle autoionize, as these states refer to Rydberg molecules built on rotationally and vibrationally excited cores.

The overall number of segments chosen in the Dalitz plots of Fig. 5 is such that the statistical error in all but two segments is below 10%, 5% being a characteristic value. As can be seen from the bottom row in Fig. 5, the error is alway highest for the segment with highest segment number. This is due to the very poor detection efficiency in the immediate vicinity of the strictly linear decay geometry (encompassed by segment[7] 45), resulting in a low event rate in this segment. There is a clear trend in the development of the Dalitz maps with total energy for the signal from field-induced dissociation.[8]

In order to indicate the significance of differences between the Dalitz plots for the different energy regions we show below each Dalitz plot the corresponding segment intensities with statistical error bars. Segment intensities are drawn saturated for values of $s > 1$. The location of the segment numbers is illustrated at the right bottom of Fig. 5. Increasing dominance of the near-linear fragment orientation appears as the total energy increases.

We find it remarkable that the results in Figs. 5(c) and 5(d) bear close resemblance to the result obtained in dissociative capture of slow electrons by H_3^+ by Strasser *et al.* [6]. To emphasize this point we compare his result (on the left of Fig. 8 in [6]) with the result which we obtain in the energy range around the ionization threshold in Fig. 6. The detailed dynamics which lead to specific Dalitz patterns remain elusive at this point. Both the geometry at which the initial state finds access into the continuum as well as the propagation of the wave packet along the repulsive potential energy surfaces

[7]In this geometry, one of the fragments stays at rest in the center-of-mass frame, thus impinging upon the beam flag.

[8]Dalitz maps obtained at zero field show no such pronounced energy dependence (not shown), which is not unexpected as dissociation then occurs over a long flight distance, thus smearing out the energy resolution and rendering the W scale a rough indicator only.

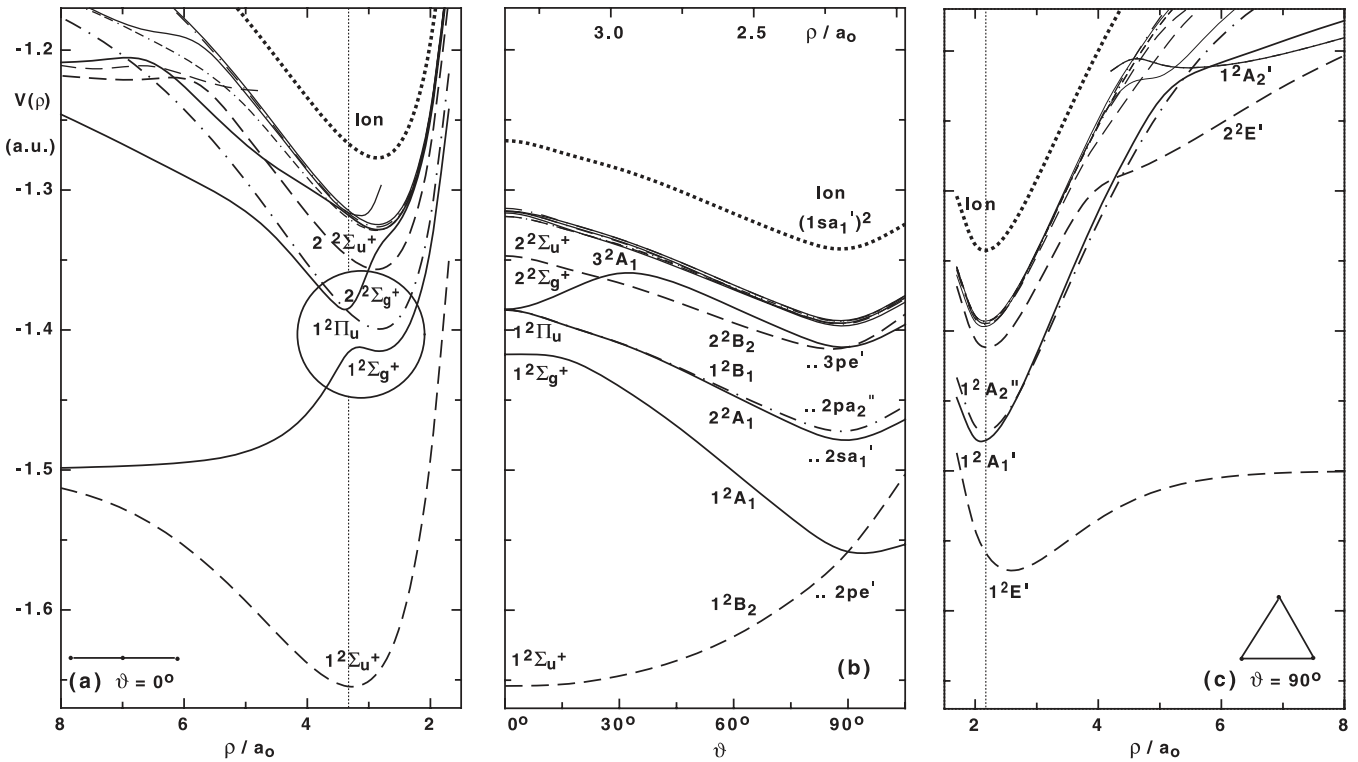

FIG. 7. Cuts through the potential surfaces of H_3. Left: $D_{\infty h}$ symmetry; center: transition conserving C_{2v} from D_{3h} to $D_{\infty h}$ (see text); right: D_{3h}. Full lines (in $D_{\infty h}$,C_{2v},D_{3h}) Σ_g^+, A_1, and A_1'; dashed Σ_u^+, B_2, and E'; dot-dashed Π_u, B_1, and A_2''. The vertical lines indicate coordinates common to the middle panel. Figure taken from Ref. [9].

TABLE I. Threshold energies based on the two-particle fragmentation energies $H_3\,3s\,A_1' \rightarrow H_2(v=0,J=1)+H(1s)$ obtained in the experiment [5].

State	Rotation	Energy (eV)
$H^+ + H_2(v=0)$	$J=0$	9.120364[a]
H_3^+ $(v_1=0,v_2=0)$	$N^+=1,K^+=1$	4.787 ± 0.015
$H_3\,3s\,A_1'$ $(v_1=0,v_2=0)$	$N=1,K=0$	3.192 ± 0.015
$H_3\,2p\,A_2''$ $(v_1=0,v_2=0)$	$N=0,K=0$	1.122 ± 0.015
$H(1s)+H(1s)+H(1s)$		0

[a]Based on the difference between 36 118.06962(37) cm^{-1} (dissociation energy of $H_2(v=0,J=0)$ [26]) and 1 09 678.7737 cm^{-1} (ionization energy of the hydrogen atom [29]).

control the center-of-mass orientation of fragment momenta in the final state. It is also clear that in both experiments the ionic core of the initial state is at the lowest ionic energies in D_{3h} geometry.

We see from the potential energy curves of Jungen [9], which we reproduce in Fig. 7, that in D_{3h} geometry no favorable access exists to the three-atom continuum (dissociation limit at -1.5 at. units). As we transit to linear geometry ($D_{\infty h}$) a series of avoided crossings of $^2\Sigma_g^+$ states appear (see the circled area and the corresponding avoided crossings at higher principal quantum numbers). At the equilibrium geometry [dashed vertical line in Fig. 7(c) and the points at 90° in Fig. 7(b)] these states merge into the degenerate npe' Jahn-Teller pairs. Kokoouline and Greene [13] showed that these states, specifically $3pe'$, are responsible for efficient dissociative electron capture. It is not unlikely that these states also steer the dissociation path of high Rydberg states and of low-energy electron capture into predominantly near-linear fragment orientation.

ACKNOWLEDGMENTS

This research was supported by Grant No. HE 2525/5 of the Deutsche Forschungsgemeinschaft. We thank Dr. Strasser for providing us with his original data and Professor Greene for drawing our attention to Refs. [24,25].

APPENDIX: REANALYSIS OF THRESHOLD ENERGIES IN H_3

The most precise experimental reference of excited states of H_3 to the energy scale of the three-particle continuum, $H(1s)+H(1s)+H(1s)$, appears to be the experiment by Galster *et al.* [5] who determined the energy release in dissociation of the ground vibrational level of $H_3\,3s\,A_1'(N=1,K=0)$ into $H_2(v,J)+H$ with rotational resolution. In this measurement the energy gap from the selected rovibronic level of the H_3 molecule to over 50 ortho states of $H_2(v,J)$ was measured (see Fig. 10 of [5]) with the combined result that

$$H_3\,3s\,A_1'(N=1,K=0) - H_2(v=0,J=1) = 7.655 \pm 0.015\text{eV}.$$

Adding the rotational spacing in $H_2(v=0)$ between $J=1$ and $J=0$ of 121.7 cm^{-1} and subtracting the experimental dissociation energy of $H_2(v=0,J=0)$ of 36 118.06962 cm^{-1} given by Liu *et al.* [26], we find that $H_3\,3s\,A_1'(N=1,K=0)$ lies 3.192 ± 0.015 eV above $H(1s)+H(1s)+H(1s)$. As the metastable level $2p\,A_2''(N=0,K=0)$ lies 16 694.972 cm^{-1} below $3s\,A_1'(N=1,K=0)$ [22], we find that $2pA_2''(N=0,K=0)$ is 1.122 eV above the three-body limit. Adding the spectroscopically known transition energy from $2p\,A_2''(N=0,K=0)$ to the first ionization limit $H_3^+(N^+=1,K^+=0)$ of 29 562.58 cm^{-1} [27] we obtain for the lowest ionization threshold of H_3 with respect to three separated hydrogen atoms the value of 4.787 $\pm$ 0.015 eV. Table I collects the pertinent energies.

The value derived for the bond dissociation energy $D_0^0(H_3^+)$ in [28] has to be revised on the basis of measurement [5]. Adding the dissociation energy of $H_2(v=0,J=0)$ of 4.478 eV [26] and using the separation between $H_3^+(N^+=1,K^+=0)$ and $H_3^+(N^+=1,K^+=1)$ of 22.84 cm^{-1}, we locate $H_3^+(N^+=1,K^+=1)$ at 9.262 eV above $H_2(v=0,J=0)+H(1s)$. Subtracting this value from the ionization energy of atomic hydrogen atom, we find $D_0^0(H_3^+)=4.336 \pm 0.015$ eV, in agreement with the latest theoretical values [24,25], which we collect in Table II.

TABLE II. Dissociation energy of $H_3^+(v_1=0,v_2=0)(N=1,K=1)$ into $H^+ + H_2(v=0,J=0)$, derived on the basis of the experimental two-particle fragmentation energy [5].

Authors	Energy (eV)
Munro *et al.* [24]	4.328
Kutzelnigg and Jaquet [25]	4.332
Reanalysis of [28] using [5]	4.336 ± 0.015

[1] A. Suzor-Weiner and I. F. Schneider, Nature (London) **412**, 871 (2001).
[2] V. Kokoouline, C. H. Greene, and B. D. Esry, Nature (London) **412**, 891 (2001).
[3] P. Cosby and H. Helm, Phys. Rev. Lett. **61**, 298 (1988).
[4] U. Müller and P. Cosby, J. Chem. Phys. **105**, 3532 (1996).
[5] U. Galster, P. Kaminski, M. Beckert, H. Helm, and U. Müller, Eur. Phys. J. D **17**, 307 (2001).
[6] D. Strasser, L. Lammich, H. Kreckel, S. Krohn, M. Lange, A. Naaman, D. Schwalm, A. Wolf, and D. Zaifman, Phys. Rev. A **66**, 032719 (2002).
[7] J. Peterson, P. Devnyck, C. Hertzler, and W. Graham, J. Chem. Phys. **96**, 8128 (1992).
[8] C. M. Laperle, J. E. Mann, T. G. Clements, and R. E. Continetti, Phys. Rev. Lett. **93**, 153202 (2004).
[9] U. Galster, F. Baumgartner, U. Müller, H. Helm, and M. Jungen, Phys. Rev. A **72**, 062506 (2005).
[10] I. Schneider and A. Orel, J. Chem. Phys. **111**, 5873 (1999).
[11] M. Lehner and M. Jungen, J. Phys. B **42**, 065101 (2009).
[12] U. Galster, Phys. Rev. A **81**, 032517 (2010).
[13] V. Kokoouline and C. H. Greene, Phys. Rev. A **69**, 032711 (2004).

[14] I. Mistrík, R. Reichle, H. Helm, and U. Müller, Phys. Rev. A **63**, 042711 (2001).
[15] U. Galster, U. Müller, and H. Helm, Phys. Rev. Lett. **92**, 073002 (2004).
[16] F. Baumgartner and H. Helm, Phys. Rev. Lett. **104**, 103002 (2010).
[17] U. Müller, T. Eckert, M. Braun, and H. Helm, Phys. Rev. Lett. **83**, 2718 (1999).
[18] G. Gellene and R. Porter, J. Chem. Phys. **79**, 5975 (1983).
[19] H. Bethe and E. Salpeter, *Quantum Mechanics of One- and Two-Electron Atoms* (Plenum, New York, 1977).
[20] C. Bordas and H. Helm, Phys. Rev. A **43**, 3645 (1991).
[21] C. Bordas, L. Lembo, and H. Helm, Phys. Rev. A **44**, 1817 (1991).
[22] I. Dabrowski and G. Herzberg, Can. J. Phys. **58**, 1238 (1980).
[23] R. H. Dalitz, Philos. Mag. **44**, 1068 (1953).
[24] J. Munro, J. Ramanlal, J. Tennyson, and H. Mussa, Mol. Phys. **104**, 115 (2006).
[25] W. Kutzelnigg and R. Jaquet, Philos. Trans. R. Soc. London, Ser. A **364**, 2855 (2006).
[26] J. Liu, E. Salumbides, U. Hollenstein, J. Koelemeij, K. Eikema, W. Ubachs, and F. Merkt, J. Chem. Phys. **130**, 174306 (2009).
[27] H. Helm, Phys. Rev. A **38**, 3425 (1988).
[28] P. Cosby and H. Helm, Chem. Phys. Lett. **152**, 71 (1988).
[29] See [http://physics.nist.gov].